King Saud University

Arabian Journal of Chemistry

www.ksu.edu.sa
www.sciencedirect.com

ORIGINAL ARTICLE

Promising extruded catalyst for palm oil transesterification from LiAlH$_4$ hydrolysates

Federico Jiménez-Cruz [a],[*], Celia Marín-Rosas [b], Luis Carlos Castañeda-Lopez [c], José Luis García-Gutiérrez [a],[*]

[a] *Instituto Mexicano Del Petróleo, Gerencia de Separación de Hidrocarburos, Eje Central Lázaro Cárdenas Norte 152, Col. San Bartolo Atepehuacan, Gustavo A. Madero, 07730 Ciudad de México, Mexico[1]*
[b] *Gerencia de Desarrollo de Materiales y Productos Químicos, Eje Central Lázaro Cárdenas Norte 152, Col. San Bartolo Atepehuacan, Gustavo A. Madero, 07730 Ciudad de México, Mexico[1]*
[c] *Gerencia de Productos para la Transformación de Crudo, Eje Central Lázaro Cárdenas Norte 152, Col. San Bartolo Atepehuacan, Gustavo A. Madero, 07730 Ciudad de México, Mexico[2]*

Abstract Transesterification catalysts prototypes of LiAlP/montmorillonite from LiAlH$_4$ hydrolysates (LiOH-Al(OH)$_3$) have been synthesized and extruded. The extruded catalysts preserve the basic structure of montmorillonite K10 according to X-ray diffraction results, which promote transesterification of triglycerides present in palm oil with methanol to generate FAMEs. Palm oil conversions of up to 89.7% were achieved in a batch reactor at 200 °C, 40 Kg/cm^2, and MeOH:Oil molar ratio of 18:1. The results obtained suggest that the good catalytic activity of the extrudates is due to the adequate combination of the Lewis acid sites and the mesoporous structure obtained during the reaction between the montmorillonite, phosphoric acid and LiOH-Al(OH)$_3$. By mean of B3LYP/6-31G* calculations, the behavior of the electrophilicity for the palm oil triglycerides and the corresponding H, Li and Al cations is remarkable, the highest electrophilicity for cation is in this order: H > Al > Li and more important for triglyceride aluminum cation in which palmitoyl moiety is in the methine carbon of glycerol moiety.

© 2021 The Author(s). Published by Elsevier B.V. on behalf of King Saud University. This is an open access article under the CC BY-NC-ND license (http://creativecommons.org/licenses/by-nc-nd/4.0/).

* Corresponding authors.
E-mail addresses: jimenezf@imp.mx (F. Jiménez-Cruz), garciajl@imp.mx (J.L. García-Gutiérrez).
[1] DITH, Instituto Mexicano del Petróleo.
[2] DTP, Instituto Mexicano del Petróleo.
Peer review under responsibility of King Saud University.

ELSEVIER **Production and hosting by Elsevier**

1. Introduction

Biodiesel, chemically the fatty acids monoalkyl esters from vegetable oil or animal fats, is a renewable, biodegradable, and clean-burning fuel that can be used instead of the petroleum diesel. The use of biodiesel is rapidly growing in many regions of the world, particularly the European Union, South America, and the United States (Chua et al., 2020). Green-

house gas emissions (hydrocarbons, CO, CO_2, SO_2) are produced in minor proportion during the combustion of biodiesel compared to fossil diesel. The world production of biodiesel increased at an annual growth rate of approximately 14.9% during the period 2006–2019 (Bockey, 2019). Biodiesel can be produced by transesterification of triglycerides from any vegetable oil or animal fat, such as soybean oil, palm oil, peanut oil, and other vegetable oils. In this context, transesterification, sometimes called alcoholysis of esters, is a reaction between triglycerides and an alcohol in the presence of a chemical or enzymatic catalyst to produce glycerol and alkyl esters of long-chain fatty acids; (Demirbas, 2008) thus, fatty acid methyl esters (FAMEs) are produced when methanol is used in the transesterification reaction, see Fig. 1.

The biodiesel transesterification process can be catalyzed by both homogeneous and heterogeneous catalyst with acid or basic properties. Sodium and potassium hydroxide are usually used as a homogeneous basic catalyst in the biodiesel industry due to its low cost and high conversion in short times that have a great impact on the economy of the process. However, for this type of catalyst the process has some drawbacks: a) It is an energy-demanding process; b) Soap is formed by free fatty acid neutralization and by triglyceride saponification (Fig. 1), which is an undesirable by-product

because it partially consumes the catalyst, decreases the biodiesel yield, and increases the viscosity by formation of gels which complicates the separation and purification steps; c) Alkaline waste-water requires treatment. Additionally, there are several factors affecting transesterification: Molar ratio of glycerides to alcohol; reaction temperature; reaction time; and the content and type of triglycerides and water, in which ester hydrolysis may be performed, see Fig. 1. The alcohols that may be used in the production of biodiesel by transesterification are methanol, ethanol, propanol, butanol, and amyl alcohol (Chua et al., 2020; Demirbas, 2008). Among these alcohols methanol and ethanol are often used, while methanol is preferred instead of ethanol due to its low cost, polarity, and shortest chain length. Moreover, methanol can react quickly with triglycerides and easily solubilize sodium hydroxide and sodium methoxide (Chua et al., 2020).

To reduce the disadvantages of homogeneous basic catalysts mentioned above, several heterogeneous catalysts for transesterification of vegetable oils have been developed and described in the literature, including zeolites, clays, insoluble metal salts of amino acids, alkaline earth metal oxides and various alkaline metal compounds supported on alumina or zeolites. The conversions obtained with these catalysts are similar to their homogeneous analogs (Chua et al., 2020).
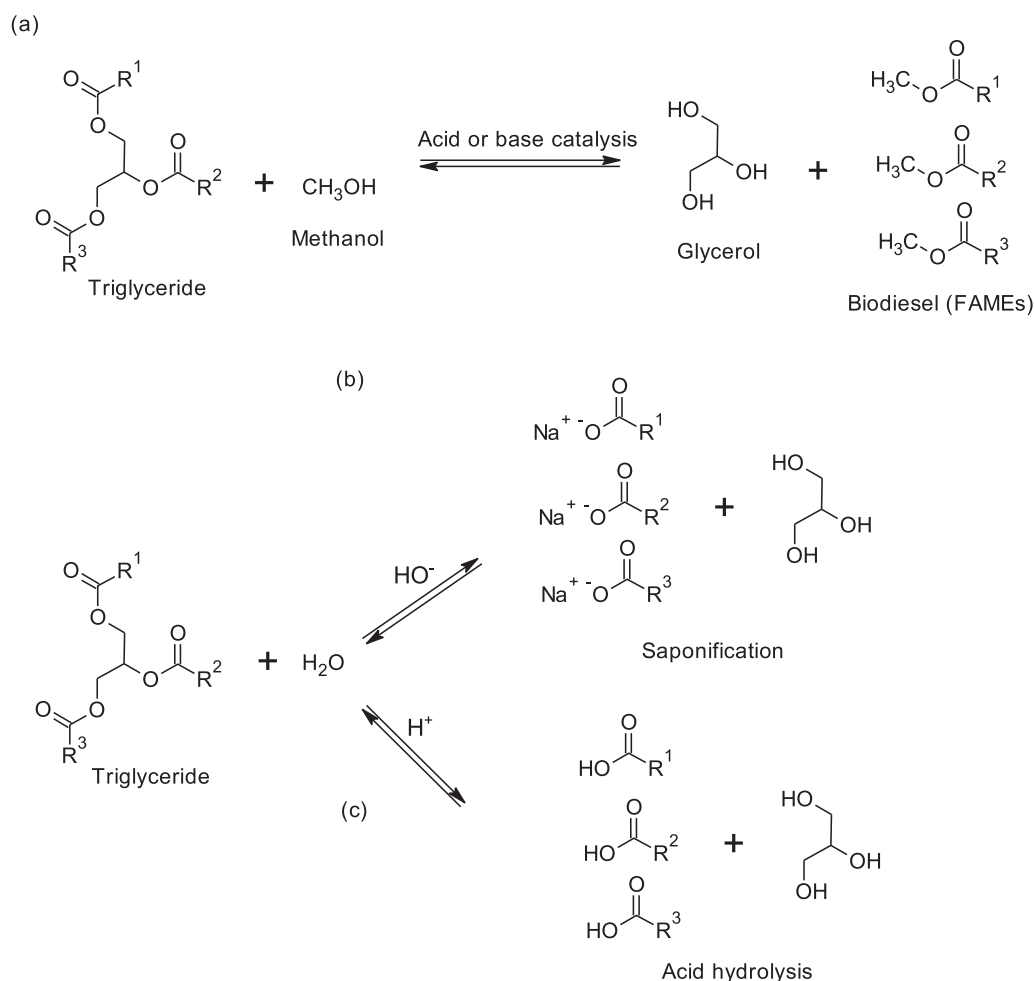
Fig. 1 Reactions of transesterification (a), saponification (b) and acid hydrolysis (c) of triglycerides.

Heterogeneous basic catalysts, such as lithium aluminum oxide, lithium metasilicate, lithium orthosilicate, and anionic clay show a very high activity for transesterification reaction, anionic clay, such as layered double hydroxide or hydrotalcite-like compound, show great potential in biodiesel production (Zhang et al., 2020).

Montmorillonite is a type of 2:1 smectite clay mineral with acidic properties, which consists of an octahedral sheet of Al^{3+} ions sandwiched between two tetrahedral sheets of Si^{4+} ions coordinated with oxygen, this arrangement of sheets forms a layer, whose ideal chemical formula is $(Al_{2-y}Mg_y)Si_4O_{10}(OH)_2 \cdot nH_2O$. The crystalline sheets present isomorphic substitution, for example, Al^{3+} and Mg^{2+} can replace Si^{4+} and Al^{3+}, respectively, which results in negatively charged aluminosilicates that are balanced by hydrated cations (Na^+, K^+ or Ca^{2+}) located in the interlayer spaces (Essington, 2004; Kaur and Kishore, 2012; Lazlo, 1987). Recently, montmorillonite clay has been studied and found to be a useful catalyst or catalyst supports in many organic reactions. Normally, reactions catalyzed by montmorillonite clay are carried out under mild conditions with good yield and selectivity towards the desired products (Kaur and Kishore, 2012). For example, it has reported the transesterification of waste cooking oil with methanol to produce FAMEs in the presence of barium-modified montmorillonite K10 catalyst was investigated in a batch reactor with conversion values of 83.4% with 3.5 wt% catalyst loading at 150 °C and methanol/oil molar ratio of 12 during a reaction time of 5 h (Olutoye et al., 2016). It has been also reported the transesterification of rapeseed oil using montmorillonite KSF as a catalyst (5 wt%), and a molar ratio of alcohol/oil = 30 at 220 °C and 53 Kg/cm^2. The conversion was 100% conversion after 4 h of reaction. However, leaching of sulfate species compromised the re-usability of this montmorillonite (Mittelbach et al., 1995).

By considering the clay properties of montmorillonite, the moderate acidity of Li and Al we propose in this investigation a catalyst based on lithium and aluminum phosphates supported on montmorillonite K10. In this context, a possible source of Li and Al can be the product of the controlled hydrolysis of lithium aluminum hydride (LAH, $LiAlH_4$), which is used as reducing reagent in organic chemistry and after quenching the excess of the reagent. The hydrolysis reaction produces hydrogen according to the following reactions: $LiAlH_4 + 4H_2O \rightarrow LiOH + Al(OH)_3 + 4H_2$, and $LiAlH_4 + 2H_2O \rightarrow LiAlO_2 + 2H_2$ (Baker and MacNevin, 1950).

The reaction is vigorously exothermic and the products have as white water homogeneous dispersion. This mixture of $LiOH + Al(OH)_3$ (LAH hydrolysates) can react with phosphoric acid (H_3PO_4) to produce lithium and aluminum phosphates.

By considering the above mentioned, in this work we present the results obtained in the development of extruded catalyst containing lithium and aluminum phosphates, and montmorillonite for palm oil transesterification. The best conversion of palm oil was 89.7%, which is higher compared with other studies carried out under similar conditions. Thus, synthesis, characterization, and evaluation of the catalysts and some discussion with the aid of DFT quantum chemical B3LYP/6-31G* calculations will be described below.

2. Experimental

2.1. General comments

Unless otherwise specified, all solvents and reagents were used without further purification: lithium aluminum hydride (LAH, Sigma-Aldrich, $LiAlH_4$, 95.0 wt%), anhydrous tetrahydrofuran (THF, Sigma-Aldrich, C_4H_8O, >99.9 wt%), phosphoric acid (Fisher Chemicals, H_3PO_4, >85 wt% in H_2O), montmorillonite K10 (Sigma-Aldrich, surface area 220–270 m^2/g), methanol (Sigma-Aldrich, >99.8 wt%), nitrogen (Praxair, 99.9 + %), deionized water, refined, bleached and deodorized (RBD) palm oil.

2.2. Characterization

The catalysts were examined by X-ray diffraction (XRD) using a Siemens diffractometer model D5000 with Cu Kα (λ = 1.5406 Å) radiation and Ni filter. The operating conditions were 35 kV and 25 mA in the angular range 4-74° in 2θ. The XRD line positions were determined with a step size of 0.02° and a counting time of 2.5 s per step.

Surface area, pore volume, and pore size distribution were determined by N_2 adsorption-desorption at -196 °C in a Micromeritics ASAP-2045 equipment using the Brunauer, Emmett and Teller (BET) method. Degasification was performed at 300 °C (See Figures S1-S5 in Supplementary information).

The acidity of the catalysts was determined via pyridine adsorption-desorption followed Fourier transform infrared (FTIR) spectroscopy using a Nicolet Portegé 460 spectrometer. The spectra were collected in the range of 4000–1000 cm^{-1}, averaging 50 scans at an instrumental resolution of 4 cm^{-1}. Prior to pyridine adsorption the sample powder was treated under vacuum at 1.33×10^{-3} Pa at 400 °C for 1 h and then cooled to room temperature. Subsequently, the sample was treated with pyridine vapor and finally heated at 300 °C under high vacuum for 1 h. FTIR spectra were collected at 50, 100 and 200 °C (See Figures S6-S8 in Supplementary information).

The proton nuclear magnetic resonance (^{1}H NMR) experiments were recorded on a Varian spectrometer at 200 MHz in deuterated chloroform (CDCl$_3$) at 25 °C. The ^{1}H chemical shifts are expressed in ppm relative to tetramethylsilane.

2.3. LAH hydrolysates preparation

In a 500 mL three-necked balloon flask was previously washed, rinsed with acetone and deionized water and dried in an oven at 115 °C for 24 h, an addition funnel was fitted in the central neck and sealed with stoppers septa was in each neck. The balloon was filled with nitrogen gas in order to generate an inert atmosphere. The reaction system was partially immersed in a circulating water bath at 0 °C. 70 mL of freshly distilled anhydrous THF was added through the addition funnel and agitation began, subsequently, 14.3 g of LAH was added in small portions to the anhydrous THF, maintaining the stream nitrogen and stirring. A 100 mL mixture of deionized water and

THF, in a volume ratio of 4:3, was prepared and placed in the addition funnel and started the addition to the LAH-THF at a rate of 1 drop per second because the reaction is very violent. (Caution! highly exothermic and hydrogen is generated). Continuous flow of N_2 through the system is necessary for allowing the gas mixture (H_2-N_2) exiting the purge to be drawn towards the hood. At the end of the addition of the deionized water: THF mixture, 150 mL of deionized water was added to the reaction mixture in slow portions by the addition funnel. The mixture obtained, LAH hydrolysates, was a white dispersion of lithium and aluminum hydroxides in water and THF, with pH = 14, which was stored in a wide-mouth bottle, tightly closed and sealed for later use.

2.4. LiAlP/montmorillonite catalyst synthesis

Concentrated H_3PO_4 in a burette was slowly added dropwise in a 100-mL beaker containing 20.0 g of LAH hydrolysates with magnetic stirring. Depending on the necessary amount of the H_3PO_4, the pH of the mixture was determined as a control of the addition, obtaining a homogenized suspension, then 8.5 g of montmorillonite K10 was added with mechanical stirring in portions of 10-fold. The obtained paste was extruded into rods of 3.1 mm in diameter and dried at room temperature for 18 h. Subsequently, the extrudates were fragmented to sizes of 3–4 cm in length and placed in a porcelain cap of 12 cm in diameter to be dried at 120 °C for 3 h and calcined at 350 °C for 4 h. Finally, the calcined extrudates were crushed and sieved for obtaining between 30 and 40 mesh particle sizes. In this way, five catalysts were synthesized with different amounts of H_3PO_4, which are named LAPMx, where "x" indicates the milliliters of acid, namely: LAPM0.4, LAPM0.7, LAPM1.3, LAPM2.2 and LAPM5.9.

2.5. Catalytic evaluation

Evaluation tests were carried out in a high-pressure batch reactor equipped with an annular catalyst basket. In a typical run, a mixture of the catalyst and the diluent (SiC, 30–40 mesh) was prepared to obtain a homogeneous solid mixture and loaded in the catalyst basket, then the basket with the catalyst was introduced into the reactor. Palm oil and methanol were weighed, then poured into the reactor vessel. The reactor was immediately sealed and fed with N_2 to an initial pressure of 7 Kg/cm^2; upon reaching this pressure the N_2 feed was suspended. The reactor was programmed for heating to reach 200 °C and the reactor controller was set at a stirring speed of approximately 750 rpm. The heating program was performed to reach 100 °C and changed the heating from 100 to 200 °C. The start of the reaction is considered when the reactor reaches 200 °C and 40 Kg/cm^2, the pressure, temperature, stirring speed, and heating are recorded every 15 min for 6 h. After 6 h of reaction, heating is stopped in the reactor controller, and the gradual cooling of the reactor is started until approximately the initial temperature and a pressure of 7 Kg/cm^2. The reactor is opened, and the oily product is centrifuged by using a centrifuge at 1500 rpm for 10 min. The phases obtained in the centrifugation are separated and the weight and volume of these phases are recorded to further per-

form the mass balance. The phase separation is carried out with Pasteur pipettes, starting the pipetting of the sample of the lower phase. Subsequently, the biodiesel phase undergoes simple distillation to remove the excess of methanol. A biodiesel sample is taken to send to NMR analysis to evaluate the conversion percentage of FAMEs. The catalyst and diluent are cleaned into a Soxhlet extractor with chloroform.

A typical run procedure consists in weighing 30.0 mg of a reaction mixture sample isolated from the reactor. Dissolve the sample with 0.8 mL of CDCl$_3$ and transfer this solution to an NMR tube using a Pasteur pipette. The process of the obtained FID was performed in the ACD Labs NMR software and proceed to extend the signals by integration which correspond to the CH$_3$ zone of the ester and the methylene group (CH$_2$) adjacent to the COOCH$_3$ ester in the reaction mixture. The determined integral values were substituted in the following expression to determine the conversion percentage (C) of FAMEs.

$$C = 100 \left(\frac{2 * Area\ CH_3}{3 * Area \alpha CH_2} \right) \qquad (1)$$

2.6. Quantum chemical calculations

All calculations were carried out using Spartan'18 (Wavefunction Inc., Irvine, CA, USA) (Spartan, 2018). To show the carbonyl electrophilic properties, the modeling of the triglyceride and the cationic models were submitted to conformational analyses at Molecular Mechanics level. Consecutively, the full optimized geometry of each molecule was performed using the hybrid of Becke's non-local three-parameter exchange and correlation functional with the Lee-Yang-Parr functional (B3LYP) level of theory with the 6-31G* basis set (Becke, 1993) by using Q-Chem (Shao et al., 2015) incorporated on Wavefunction Spartan'18.

3. Results and discussion

3.1. Catalyst synthesis and characterization

The reaction of concentrated H_3PO_4 and the LAH hydrolysates depending on the pH of the mixture in which the phosphates species are present in the different equilibrium reactions:

$$H_3PO_4 \leftrightarrows H^+ + {}^-H_2PO_4 \ (pKa = 2.12) \qquad (2)$$

$${}^-H_2PO_4 \leftrightarrows H^+ + {}^{-2}HPO_4 \ (pKa = 7.21) \qquad (3)$$
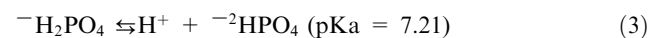
Table 1 H_3PO_4 added to LAH hydrolysates.

Catalyst	H_3PO_4 mL	mmol	Final pH
LAPM0.4	0.4	5.8	12
LAPM0.7	0.7	9.5	9
LAPM1.3	1.3	19.0	5
LAPM2.2	2.2	32.2	3
LAPM5.9	5.9	86.2	1
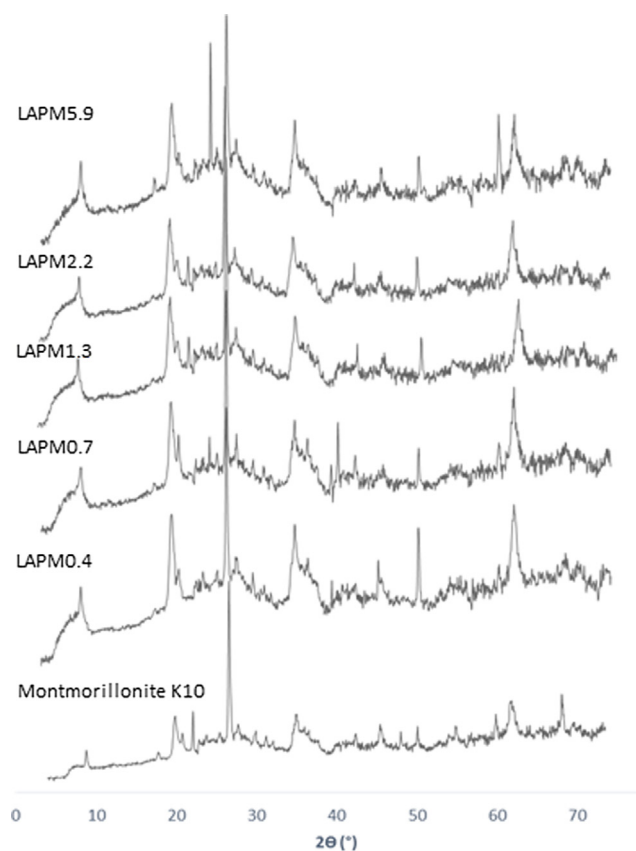
Fig. 2 XRD pattern for montmorillonite K10 and extruded catalysts.

$$^{-2}HPO_4 \leftrightarrows H^+ + {^{-3}PO_4} \quad (pKa = 12.3) \qquad (4)$$

As is depicted in Table 1 during the H_3PO_4 addition, we selected five pH samples to prepare five catalysts. The product of each lithium and aluminum phosphates were mixed with the montmorillonite as previously mentioned.

The X-ray diffraction pattern of the montmorillonite K10 and prepared catalysts is shown in Fig. 2. The clay exhibits typical diffraction peaks previously reported (Bharadwaj et al., 2014; Ibrahim et al. 2018) (PDF 3-0015) at 7.9, 19.1 and 34.5°. The peaks at 20.3, 26.6, 50.4 and 60.0° are attributed to quartz (PDF 78-2315), while the peak at 21.8 and 61.8° is a characteristic diffraction peak of mica (ICDD 78-1928)

Table 2 Textural properties for catalysts and montmorillonite K10.

Sample	Surface area, m^2/g	Total pore volume, cm^3/g	Pore diameter, Å
Montmorillonite K10	222.0	0.31	54.0
LAPM0.4	137.0	0.25	73.4
LAPM0.7	170.7	0.29	67.0
LAPM1.3	170.4	0.29	68.9
LAPM2.2	20.9	0.03	102.6
LAPM5.9	15.3	0.04	116.8

and the peak at 27.6° is ascribed to albite (PDF 41-1480). The LAPM5.9 catalyst presents an additional signal at 24.2°, which is assigned to petalite (JCPDS 005-0381), the origin of this compound is established later. XRD pattern of the prepared catalysts and the Montmorillonite K10 are very similar. Thus, it can be concluded that the preparation of the catalysts does not destroy the porous network of montmorillonite K10.

The textural properties of the clay and catalysts synthetized are showed in Table 2. Montmorillonite K10 has a BET surface area of 222 m^2/g and a total pore volume of 0.31 cm^3/g and an average pore diameter of 54 Å. In the case of catalysts, the first two properties decreased, the decrease being very drastic for catalysts prepared with high amounts of phosphoric acid, while the average pore diameter increased markedly to 116.7 Å according to the following order: LAPM5.9≫LAPM0.7 > LAPM0.4 (See Figures S1-S5 in Supplementary information). These textural changes may be due to the agglomeration of the clay layers and the obstruction of their interlayer spaces by lithium and aluminum phosphates, which is explained later.

It is known that montmorillonite has both Brønsted and Lewis acid sites, but the treatment of this clay with mineral acids modifies the number and type of acidic sites (Pergher et al., 1999). Furthermore, commercial acid-activated montmorillonite (K10) has more Brønsted acid sites than Lewis acid sites (Nascimento et al., 2015). Thus, in order to know more about of some selected catalysts, its acid properties were determined by pyridine adsorption-desorption followed by FTIR spectroscopy (Table 3). Montmorillonite K10 shows weak and medium Lewis acid sites, the weak acid sites decrease significantly with an increase of temperature from 50 to 100 °C, and the number of medium Lewis acid sites is low at 200 °C. The clay K10 does not show Brønsted acidity by pyridine adsorption under our experimental conditions, which may be because the number of Brønsted acid sites sharply decreased during clay conditioning at 400 °C (Tichit et al., 1985). In comparison, the prepared catalysts show a lower number of weak Lewis acid sites than the clay K10, according to the following order: Montmorillonite K10 ≫ LAPM0.4 > LAPM0.7 ≫ LAPM5.9 at 50 °C, the Lewis acidity shows a similar behavior at 100 °C. Interestingly, the LAPM0.4 and LAPM0.7 samples show a higher number of medium Lewis acid sites than the clay K10 and the LAPM5.9 sample at 200 °C, that is, LAPM0.4 ≫ LAPM0.7 > , K10 > LAPM5.9. In addition to Lewis acid sites, LAPM0.7 and LAPM5.9 samples also have a very low number of weak and medium Brønsted acid sites (See Figures S6-S8 in Supplementary information).

Therefore, according to the aforementioned, we suggest that during the preparation of the catalysts the following processes may achieve:

(1) Firstly, phosphoric acid reacts with lithium hydroxide to form phosphate, monohydrogen and dihydrogen phosphates of lithium, these phosphates acting as a binder for the catalyst components by reacting with the hydroxyl groups from montmorillonite K10 (Iwamoto and Grimblot, 2000). Moreover, the phosphate-bound lithium metal can act as a Lewis acid. Finally, aluminum hydroxide can also react with phosphoric acid to give amorphous aluminum phosphate, this phosphate also exhibits Lewis acidity through the aluminum atom (Snoeyink and Jenkins, 1980).

Table 3 Brønsted and Lewis sites of selected catalyst.

μmoles Pyridine/g

Temperature (°C)	Montmorillonite K10		LAPM0.4		LAPM0.7		LAPM5.9	
	Brønsted	Lewis	Brønsted	Lewis	Brønsted	Lewis	Brønsted	Lewis
50	0	786	0	291	5	251	9	34
100	0	149	0	50	2	16	9	15
200	0	4	0	12	1	6	6	1

(2) Montmorillonite K10 in an aqueous medium can generate a pH of about 3.8, in which the Al(OH)$_3$ is present in an appreciable amount as Al^{3+} cations (Essington, 2004). The presence of an excess of Al^{3+} cations may promote the formation of some moderate Lewis acid sites by isomorphic substitution of Si^{4+} by Al^{3+} in the tetrahedral sheets (Essington, 2004; Lazlo, 1987), the incipient pillaring of the clay (Occelli and Tindwa, 1983; Bagshaw and Cooney, 1993; Ming-Yuan et al., 1988; Auer and Hofmann, 1993), and/or the replace the Ca^{2+}, Mg^{2+}, K$^+$, Na$^+$ cations, etc. found in the interlayer spaces (Huang et al., 2017). The Brønsted acidity in the catalysts is mainly associated with the hydrated cations in the interlayer spaces of montmorillonite.

(3) During the synthesis of the catalysts under highly acidic conditions, phosphoric acid in excess, Brønsted acid sites increases because of an increased number of broken edges (broken layers) and Lewis acid sites decreased due to the removal of Al^{3+} ions from octahedral sites of montmorillonite accompanied by silica formation (Madejova et al., 2009; Shinoda et al., 1995). It should be mentioned that the interaction between SiO$_2$ and Li$^+$ and Al^{3+} ions in acidic aqueous medium and subsequent heating has formed the lithium aluminosilicate (petalite) observed by XRD in LAPM5.9 catalyst (Barrer and White, 1951).

Based on the above observations, the medium Lewis acid sites on montmorillonite K10 seem to be mainly responsible for a better activity of the catalysts for transesterification (see Section 3.3), where the presence of electronegative phosphate species bonded on the tetrahedral sheets of Si would help withdraw electron density from the Lewis acid site environment, thereby conferring a higher acidity (electrophilic character) to the Al atom (Burch et al., 1998; Morterra et al., 1995).

3.2. Characterization of palm oil and reaction products

In Fig. 3 is showed the ^{1}H NMR spectrum of palm oil, in which each signal (δ, ppm) define featured moieties of fatty acids; thus, in 5.15–5.40 ppm are assigned to CH=CH double bond moieties of unsaturated fatty acids, 5.20–5.25 corresponds to CH in the glycerol moiety, 4.15–4.40 ppm is assigned to CH$_2$ in glycerol moiety, in 2.75 ppm are assigned to —CH=CH—CH$_2$—CH=CH moieties, in 2.25–
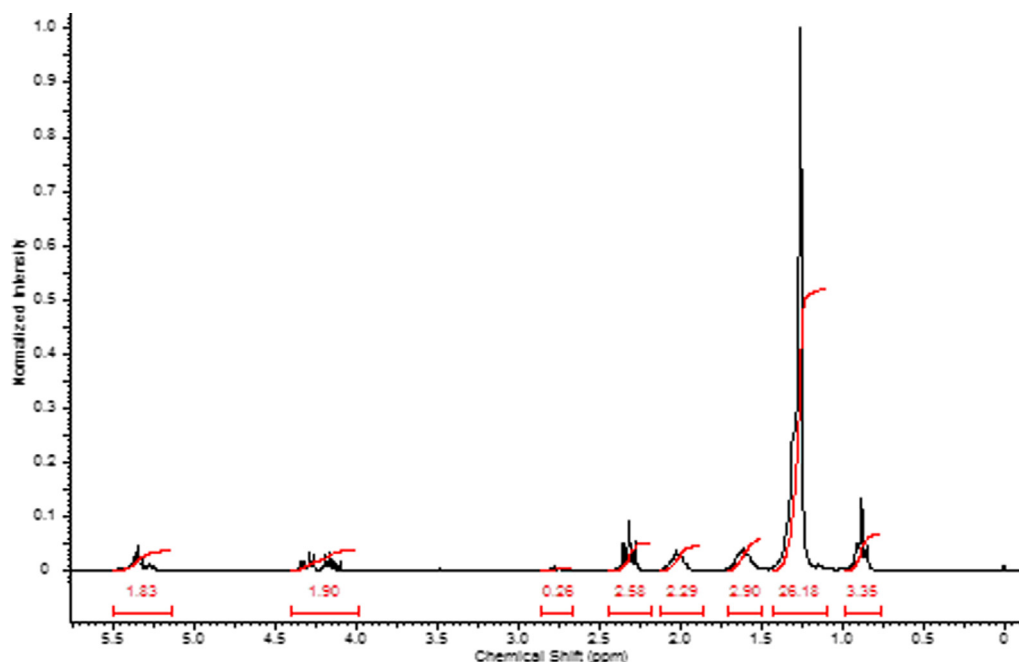
Fig. 3 ^{1}H NMR spectrum of palm oil.
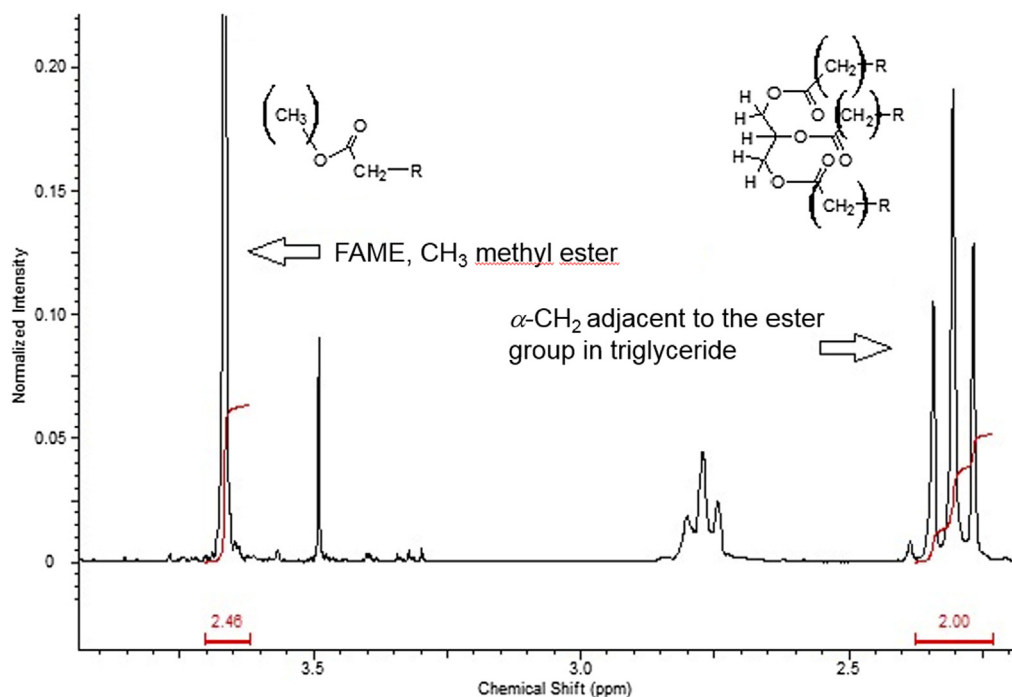
Fig. 4 ^{1}H NMR spectrum for the methyl ester and methylene adjacent to the ester group in the reaction product mixture.

Table 4 Properties of palm oil (Tan et al., 1981).

Density at 50 °C, g/mL		0.888–0.889
Kinematic viscosity at 40 °C, cSt		1.9–6.0
Acid value, mg KOH/g		0.5–0.8
Iodine value (Wijs' method), cg I_2/g.		46–56
Fatty acid composition (as methyl esters), wt%		
Lauric	C12:0	0.1–1.0
Myristic	C14:0	0.9–1.5
Palmitic	C16:0	41.8–46.8
Sapienic and Palmitoleic	C16:1	0.1–0.3
Stearic	C18:0	4.5–5.1
Oleic	C18:1	37.3–40.8
Linoleic	C18:2	9.1–11.0
Linolenic	C18:3	0.4–0.6
Arachidic	C20:0	0.2–0.7
Diglycerides, wt%		3.0–7.6

2.45 ppm is assigned to CH_2 adjacent to COO—moieties, 1.95–2.20 ppm is assigned to CH_2 adjacent to —CH=CH—, 1.50–1.70 ppm is assigned to CH_2 adjacent to CH_2—COO— moiety. In 1.20–1.40 pδpm is assigned to CH_2 in the chain and 0.80–0.90 ppm corresponds to CH_3— moiety of the chains.

The conversion percentage of FAMEs from the transesterification product was determined by ^{1}H NMR. According to the reaction, we determined the ^{1}H NMR spectrum, in which the zone from 2 to 4 ppm is carried out by identifying the triplet defined in 2.23–2.38 ppm represents the 2H of α-CH_2 adjacent to the ester group in triglyceride, meanwhile, the singlet described in the interval from 3.62 to 3.70 ppm represents the CH_3 of methyl ester in the FAMEs product (Knothe, 2006; Knothe and Kenar, 2004). Fig. 4 depicts those described above.

Mainly, palm oil is characterized by a higher content of palmitic acid esters (41.8–46.8 wt%) oleic acid esters (37.3–40.8 wt

Table 5 Evaluation conditions and conversion for palm oil transesterification with extruded catalysts.

Catalyst	LAPM0.4	LAPM0.7	LAPM1.3	LAPM2.2	LAPM5.9
Reaction time, h	6	6	6	6	6
Reaction temperature, °C	200	200	200	200	200
Pressure, Kg/cm^2	40	40	40	40	40
MeOH:Oil, mol:mol	18:1	18:1	18:1	18:1	18:1
Catalyst, g	3.2	3.2	3.2	3.2	3.2
Diluent, g	37.4	37.4	37.4	37.4	37.4
Palm oil, g	37.6	36.8	54.5	39.8	38.5
Methanol, g	25.6	25.0	37.1	27.0	26.2
Conversion (NMR, %)	89.7	88.0	82.0	65.7	44.3
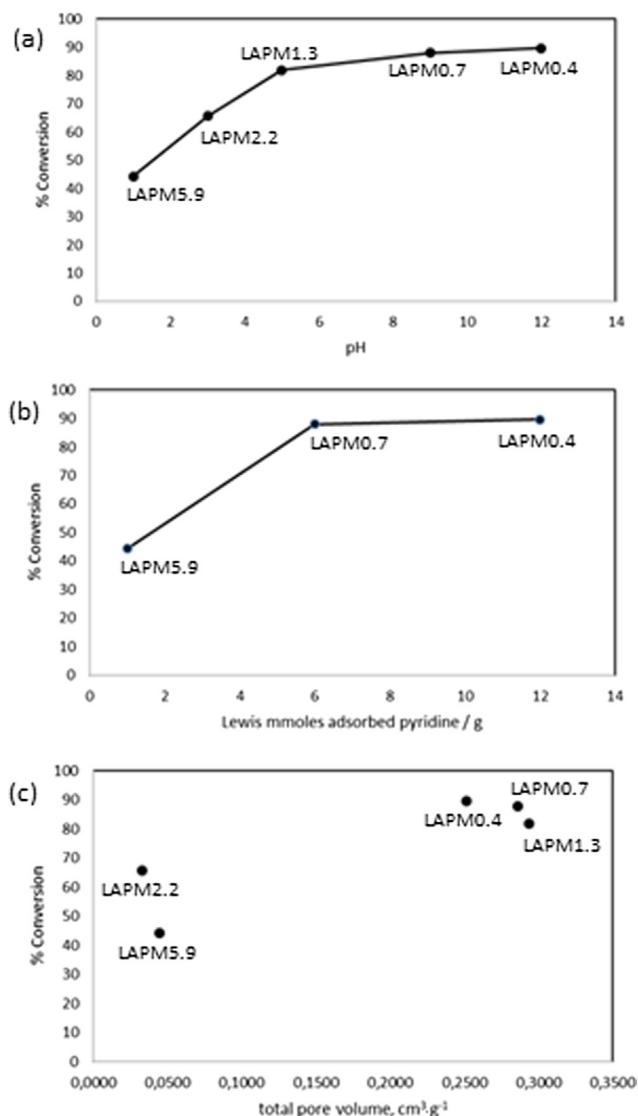
Fig. 5 Palm oil conversion in function of the synthesis pH of catalysts (a), Lewis acidity of catalysts (b), and pore volume of catalysts (c).

%) and in minor proportion of linoleic acid esters (9.1–11.0 wt %). In Table 4 are depicted the physical properties of the palm oil and typical fatty acids composition.

3.3. Catalyst evaluation in palm oil-methanol transesterification

According to the catalyst experiments evaluation described in the experimental section, the evaluation reaction temperature was performed at 200 °C, 40 Kg/cm^2 pressure, and MeOH: Oil molar ratio of 18:1 for 6 h. Table 5 shows the evaluation conditions and the conversion percentage by NMR for the transesterification reaction.

The effect of the acid properties is strong remarkable in the conversion percentage. In Fig. 5 is described this behavior. In Fig. 5a, the higher conversions are observed in the catalysts derived from lesser quantities of H$_3$PO$_4$ added to the LAH hydrolysates, corresponding to LAPM0.4, LAPM0.7,

and LAPM1.3 catalysts. By comparing the Lewis acidity of LAPM0.4, LAPM0.7, and LAPM5.9 catalysts, in Fig. 5b this behavior is also evident. In Fig. 5c, higher total pore volumes assure higher conversion to FAMEs, as is observable in LAPM0.4, LAPM0.7, and LAPM1.3 catalysts. A combination of acidity and pore access can be the key point for the transformation. It should be noted that the LAP0.4 catalyst showed after 15 runs under the same reaction conditions a decrease of 6.8% in the conversion to FAME concerning the first run.

3.4. DFT quantum chemical calculations

According to the literature, the acid properties, H$^+$ in Brønsted or metal (Li or Al) in Lewis sites can promote the interaction with the oxygen in carbonyl and enhancing the electrophilicity of the carbonyl facilitating the methanol attack

(a)

1 = R^{1}CO: Palmitoyl (P).
R^{2}CO: Linoleoyl (L).
R^{3}CO: Oleoyl (O).

2 = R^{1}CO: Linoleoyl (L).
R^{2}CO: Palmitoyl (P).
R^{3}CO: Oleoyl (O).

3 = R^{1}CO: Palmitoyl (P).
R^{2}CO: Oleoyl (O).
R^{3}CO: Linoleoyl (L).

(b)

X: H$^+$, Li$^+$, $^+$Al
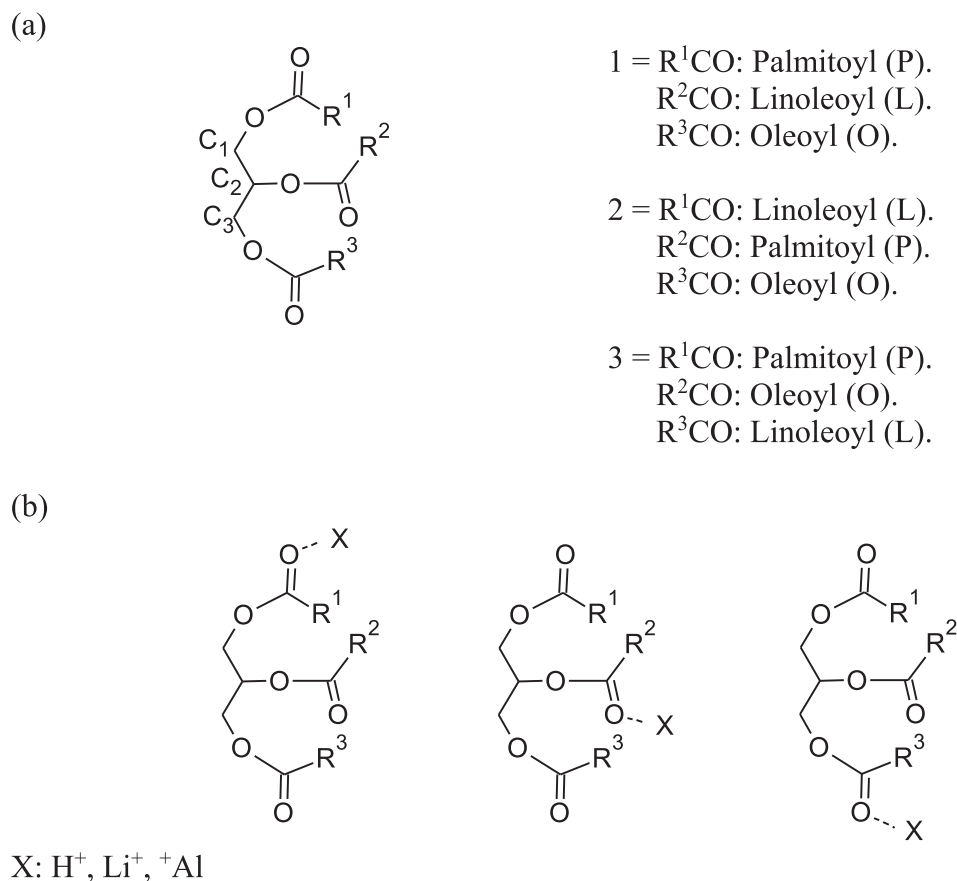
Fig. 6 Triglyceride models 1, 2, and 3 (a) used to construct the cationic models (b) in the B3LYP/6-31G* calculations.

Table 6 Gas-phase FMO properties of palm oil triglycerides and the H, Li, and Al cations.

Entry	Energy, kJ/mol	E_{HOMO}, eV	E_{LUMO}, eV	Electrophilicity (ω), eV	Hardness (η), eV	Global softness (S), 1/ev	Chemical potential (μ), eV
1	−2607.490767	−6.36	−0.03	1.61	3.17	0.32	−3.20
2	−2607.501308	−6.31	0.17	1.45	3.24	0.31	−3.07
3	−2607.493035	−6.26	−0.09	1.63	3.09	0.32	−3.18
1-PH	−2607.849486	−7.25	−5.43	22.09	0.91	1.10	−6.34
1-LH	−2607.847683	−7.39	−5.49	21.83	0.95	1.05	−6.44
1-OH	−2607.846529	−7.38	−5.36	20.09	1.01	0.99	−6.37
1-PLi	−2614.917406	−7.22	−4.29	11.30	1.47	0.68	−5.76
1-LLi	−2614.916499	−7.36	−4.26	10.89	1.55	0.65	−5.81
1-OLi	−2614.917087	−7.22	−4.29	11.30	1.47	0.68	−5.76
1-PAl	−2849.753236	−7.26	−4.84	15.13	1.21	0.83	−6.05
1-LAl	−2849.756180	−7.37	−4.94	15.59	1.22	0.82	−6.16
1-OAl	−2849.754143	−7.24	−4.91	15.84	1.17	0.86	−6.08
2-LH	−2607.851696	−7.58	−5.48	20.31	1.05	0.95	−6.53
2-PH	−2607.851044	−7.53	−5.53	21.32	1.00	1.00	−6.53
2-OH	−2607.858453	−7.43	−5.14	17.25	1.15	0.87	−6.29
2-LLi	−2614.916275	−7.44	−4.13	10.11	1.66	0.60	−5.79
2-PLi	−2614.886557	−7.34	−4.82	14.67	1.26	0.79	−6.08
2-OLi	−2614.906899	−7.49	−4.10	9.91	1.70	0.59	−5.80
2-LAl	−2849.757884	−7.52	−4.86	14.40	1.33	0.75	−6.19
2-PAl	−2849.730222	−7.41	−5.85	28.18	0.78	1.28	−6.63
2-OAl	−2849.751980	−7.48	−4.95	15.27	1.27	0.79	−6.22
3-PH	−2607.848522	−7.42	−5.54	22.34	0.94	1.06	−6.48

Table 6 (*continued*)

Entry	Energy, kJ/mol	E_{HOMO}, eV	E_{LUMO}, eV	Electrophilicity (ω), eV	Hardness (η), eV	Global softness (S), 1/ev	Chemical potential (μ), eV
3-OH	−2607.852852	−7.41	−5.57	22.89	0.92	1.09	−6.49
3-LH	−2607.847973	−7.43	−5.40	20.27	1.02	0.99	−6.42
3-PLi	−2614.918323	−7.48	−3.97	9.34	1.76	0.57	−5.73
3-OLi	−2614.914326	−7.44	−4.13	10.11	1.66	0.60	−5.79
3-LLi	−2614.928179	−7.48	−3.94	9.21	1.77	0.56	−5.71
3-PAl	−2849.755719	−7.35	−4.74	14.00	1.31	0.77	−6.05
3-OAl	−2849.749156	−7.37	−4.94	15.59	1.22	0.82	−6.16
3-LAl	−2849.754386	−7.44	−4.92	15.16	1.26	0.79	−6.18
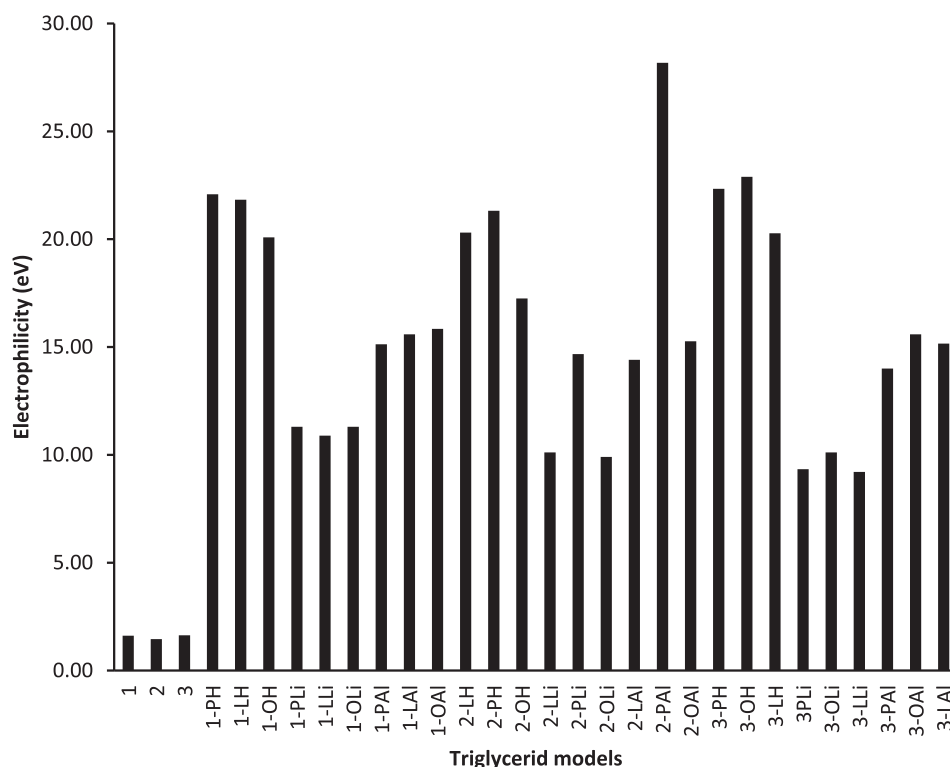
Fig. 7 Graphic comparison of electrophilicity in palm oil triglycerides 1, 2, 3, and their corresponding H, Li, and Al cations.

in the transesterification. Thus, with the aid of DFT quantum chemical calculation, we can clear this behavior.

The main components in palm oil are palmitic acid esters > oleic acid esters > linoleic acid esters in minor proportion (Table 4). Our triglycerides model considers a randomized triesters depicted in Fig. 6. The triglyceride models 1, 2 and 3 can be used to construct the cationic models to show the frontier molecular orbital (FMO) properties of the electrophilic C=O by considering proton (H$^+$), lithium cation (Li$^+$) and aluminum cation (Al$^+$). 1-PH model corresponds to a protonated triester 1 in the palmitoyl moiety, 1-PLi model corresponds to lithium cationic triester 1 in the palmitoyl moiety, and in the same manner for the other cationic models.

The constructed molecular models for the triglycerides and the corresponding cations were performed in an equilibrium geometry calculation at B3LYP/6-31G* level of theory as described above.

Calculated FMO properties for the palm oil triglyceride 1, 2, 3, and the H, Li and Al cations are described in Table 6. The total energy of a system is composed of the internal, potential, and kinetic energies for these parameters. In agreement with the FMO theory, chemical to donate reactivity is a function of the interaction between HOMO and LUMO of the reacting species (Fukui, 1975). E_{HOMO} indicates the ability of molecule electrons to an appropriate acceptor with empty molecular orbitals and E_{LUMO} measures its ability to accept electrons.
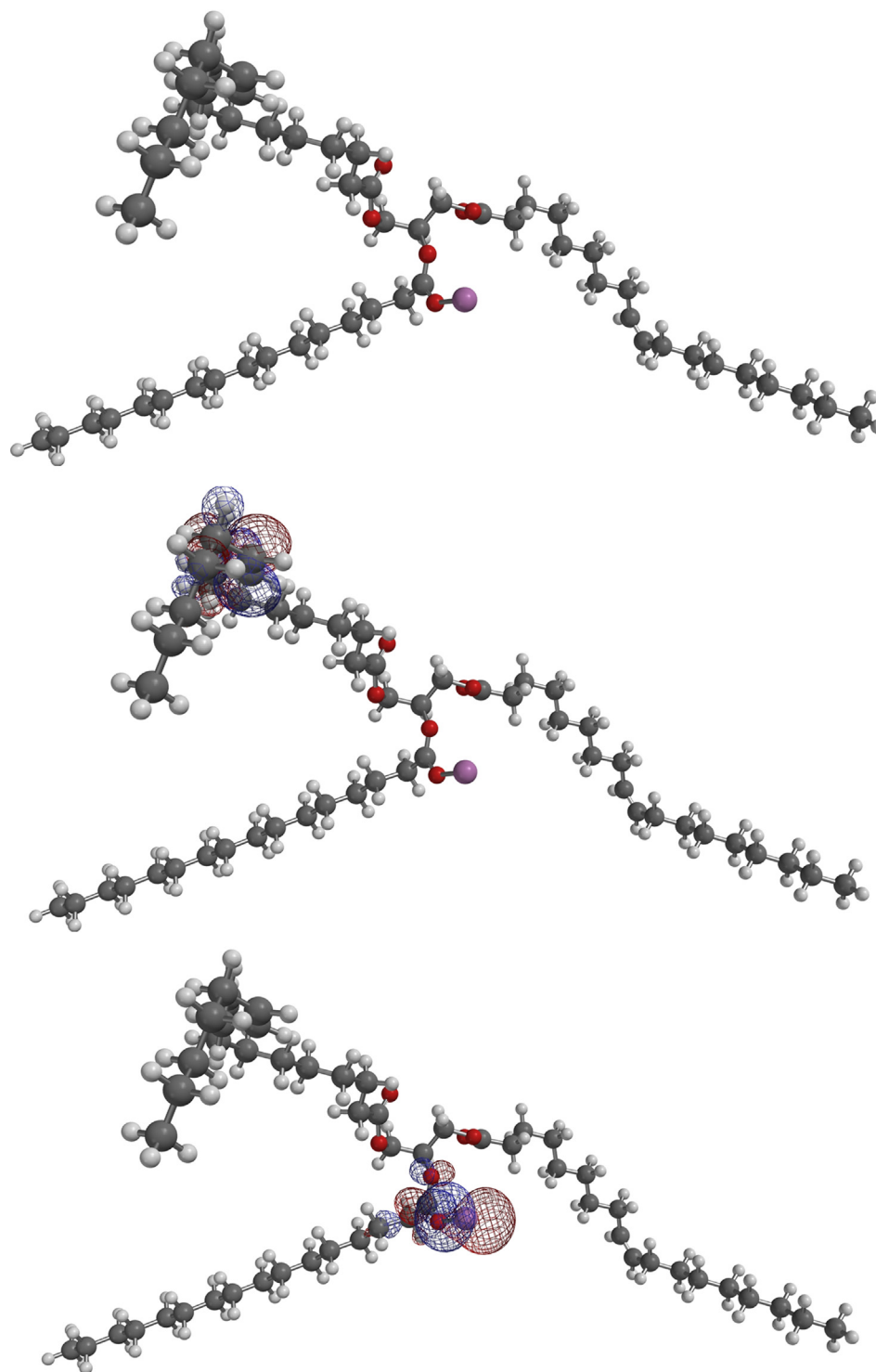
Fig. 8 Equilibrium geometry, HOMO and LUMO plots for 2-PAL model, aluminum palmitoyl moiety cation in the C-2 on glycerol moiety.

The lower the value of E_{LUMO}, the greater the ability of a molecule to accept electrons. From Table 6, it is evident that the E_{HOMO} for the palm oil triglyceride models is greater than the cationic H, Li, and Al models. In the case of the E_{LUMO}, the values for cationic models are lower than the corresponding triglycerides, this could be attributable to the nature of the

ability for electron acceptance by increasing the electrophilic carbonyl assisted by the H, Li and Al cations.

Absolute hardness (η) and softness (S) are important properties in measuring the molecular stability and reactivity. A hard molecule has a large energy gap and a soft molecule has a small energy gap. Soft molecules are more reactive than
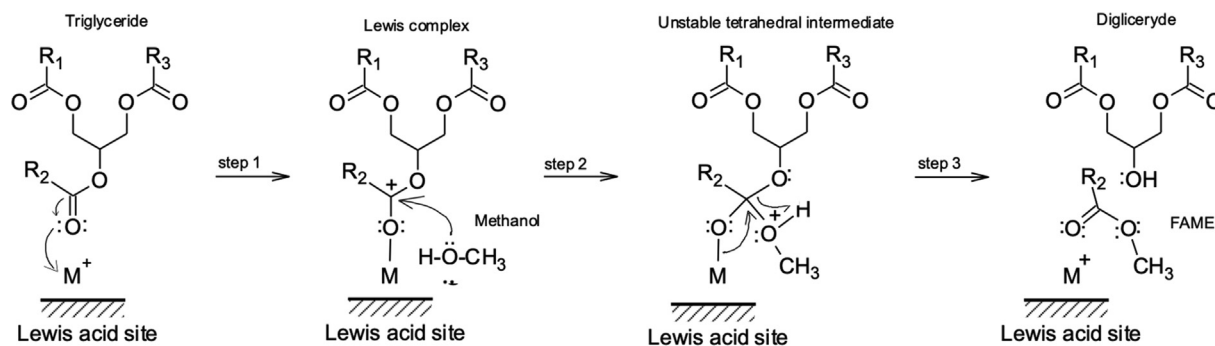
Fig. 9 Mechanism for triglyceride transesterification by Lewis acid catalysts.

hard ones because they can easily offer electrons to an acceptor. For the simplest transfer of electrons, adsorption could occur at the part of the molecule where softness, which is a local property, has the highest value.

Chemical potential (μ) measures the tendency of electrons to flow from high potential regions to low potential ones until reaching a constant state (Parr et al., 1999). Table 6 summarized the values of μ for non-cationic and cationic triglyceride models, being the non-cationic.

The electrophilicity (ω) is a property in which a chemical species has the ability to be electrophilic reagents by accepting electrons from nucleophiles to form new bonds, the calculation is developed by Parr et al. (Parr et al., 1999). According to Table 6 the electrophilicity can be calculated from chemical potential and hardness values according to the next expression: $\omega = \mu^2/2\eta$. In Fig. 7 is depicted the behavior of the electrophilicity for the palm oil triglycerides 1, 2, 3 and the corresponding H, Li and Al cations; it is remarkable that the highest electrophilicity for cation in this order: H > Al > Li and more important for triglyceride 2 cations in which palmitoyl moiety is in the methine carbon of glycerol moiety (central C2 of the triglyceride).

Fig. 8 shows the equilibrium geometries for 2-PAL, aluminum palmitoyl moiety cation in the C-2 on glycerol moiety and the corresponding highest occupied molecular orbital (HOMO) and lowest unoccupied molecular orbital (LUMO) localized sites.

It is well-known that the first attack of the methanol nucleophile to the protonated or cationic metal carbonyl in the triglyceride is the central C2 achieving the first ester cleavage in the transesterification reaction. Li and Al in the catalyst series LAPM0.4 to −5.9 have a good promotion for the reaction because of the presence of the lithium and aluminum phosphates with the aid of some Brønsted sites (H$^+$) and the appropriate textural mesoporous montmorillonite clay support.

3.5. Transesterification mechanism by Lewis acid catalyst

According to the literature, heterogeneous acid catalysts could be classified as Lewis or Brønsted acid catalysts, of which Lewis acid catalysts have greater transesterification activity than Brønsted acid catalysts (De et al., 2016; Hanif et al., 2017). In this context, a single site reaction mechanism, Eley-Rideal (ER) type, has been suggested for transesterification

by Lewis acid catalysts in which the carboxyl of triglyceride is adsorbed to the catalyst active site and the alcohol reacts with it directly from the fluid phase.

On other hand, taking into account the results obtained, that is, the highest conversion of palm oil is obtained with the catalyst LAPM0.4, which only presents acidic sites of Lewis, and the calculated FMO properties for the palm oil triglyceride, we show a chemical mechanism, which is explained in detail below, Fig. 9 (De et al., 2016; Hanif et al., 2017).

As a first step, the coordination of triglyceride in the catalyst site. The oxo-type oxygen atom of triglyceride interacts with a Lewis acid site of the catalyst due to electrophilic property, this rate-determining step depends on the number and strength of acid sites in the catalyst. The newly formed Lewis complex has a more electrophilic carbon in the carboxyl of the triglyceride. The second step is the intermolecular attack of methanol (a weak nucleophile) on the electrophilic carbon which creates an unstable tetrahedral intermediate. The third step is breaking of unstable tetrahedral intermediate to FAME and diglyceride by back donating of the electron pair on the initial oxo-type oxygen to the adjacent tetrahedral carbon atom, the breaking bond between the protonated ester and the corresponding alkoxide of the diglyceride, and proton transfer between these two species. In this last step the strength of Lewis acid sites is very important, since very strong acidity does not allow product formation.

So, the three steps are repeated for each fatty acid alkyl ester production, that is, the triglyceride is converted stepwise to di- and monoglyceride and finally glycerol.

4. Conclusions

Promising prototypes of LiAlP/montmorillonite catalysts LAPM-0.4 to −5.9 from LiAlH$_4$ hydrolysates (LiOH-Al(OH)$_3$) have been developed. The extruded catalysts have mainly the structure of montmorillonite K10 according to X-ray diffraction determination, having majorly Lewis acid sites and pore size appropriate to promote transesterification of triglycerides present in palm oil with methanol to generate FAMEs. Palm oil conversions of up to 89.7% were achieved in a batch reactor at 200 °C, 40 Kg/m^2, and MeOH:Oil molar ratio of 18:1 during 6 h. The results obtained suggest that the good catalytic activity of the extrudates is due to the adequate combination of the Brønsted acid sites and the mesoporous

structure provided by lithium and aluminum phosphates and montmorillonite, respectively. By B3LYP/6-31G* calculations quantum calculations, the behavior of the electrophilicity for the palm oil triglycerides and the corresponding H, Li and Al cations is remarkable, the highest electrophilicity for cation is in this order: H > Al > Li and more important for triglyceride aluminum cation in which palmitoyl moiety is in the methine carbon of glycerol moiety.

Declaration of Competing Interest

The authors declare that they have no known competing financial interests or personal relationships that could have appeared to influence the work reported in this paper.

Acknowledgements

Appendix A. Supplementary material

Supplementary data to this article can be found online at https://doi.org/10.1016/j.arabjc.2021.103141.

References

Auer, H., Hofmann, H., 1993. Pillared clays: characterization of acidity and catalytic properties and comparison with some zeolites. Appl. Catal. A Gen. 97, 23–38. https://doi.org/10.1016/0926-860X(93)80064-W.

Bagshaw, S.A., Cooney, R.P., 1993. FTIR surface site analysis of pillared clays using pyridine probe species. Chem. Mat. 5 (8), 1101–1109. https://doi.org/10.1021/cm00032a013.

Baker, B.B., MacNevin, W.M., 1950. Lithium Aluminum Hydride as Reagent for Determination of Water. Anal. Chem. 22, 364–365. https://doi.org/10.1021/ac60038a044.

Barrer, R.M., White, E.A.D., 1951. The hydrothermal chemistry of silicates. Part I. Synthetic lithium aluminosilicates. J. Chem. Soc., 1267–1278 https://doi.org/10.1039/JR9510001267.

Becke, A.D., 1993. Density-functional thermochemistry. III. The role of exact exchange. J. Chem. Phys. 98, 5648–5652. https://doi.org/10.1063/1.464913.

Bharadwaj, S.K., Boruah, P.K., Gogoi, P.K., 2014. Phosphoric acid modified montmorillonite clay: A new heterogeneous catalyst for nitration of arenes. Catal. Commun. 5, 124–128. https://doi.org/10.1016/j.catcom.2014.08.019.

Bockey, D., 2019. The significance and perspective of biodiesel production – A European and global vie. Oilseeds & fats Crops and Lipids. OCL 26, 40. https://doi.org/10.1051/ocl/2019042.

Burch, R., Holpin, E., Hayes, M., Ruth, K., Sullivan, J.A., 1998. The nature of activity enhancement for propane oxidation over supported Pt catalysts exposed to sulphur dioxide. Appl. Catal. B Environ. 19, 199–207. https://doi.org/10.1016/S0926-3373(98)00079-4.

Chua, S.Y., Periasamy, L.A.P., Goh, C.M.H., Tan, Y.H., Mubarak, N.M., Kansed, J., Khalid, M., Walvekar, R., Abdullahd, E.C., 2020. Biodiesel synthesis using natural solid catalyst derived from biomass waste - A review. J. Ind. Eng. Chem. 81, 41–60. https://doi.org/10.1016/j.jiec.2019.09.022.

De, S., Dutta, S., Saha, B., 2016. Critical design of heterogeneous catalysts for biomass valorization: current thrust and emerging. Catal. Sci. Technol. 6, 7364–7385. https://doi.org/10.1039/C6CY01370H.

Demirbas, A., 2008. Biodiesel: A Realistic Fuel Alternative for Diesel Engines. Springer, London.

Essington, M.E., 2004. Soil and Water chemistry. An integrative approach. CRC Press, United States of America.

Fukui, K., 1975. Theory of Orientation and Stereoselection. Springer-Verlag, New York.

Hanif, M.A., Nisar, S., Rashid, U., 2017. Supported solid and heteropoly acid catalysts for production of biodiesel. Catal. Rev. 59, 165–188. https://doi.org/10.1080/01614940.2017.1321452.

Huang, X., Chen, L., Ren, F., Yang, C., Li, J., Shi, K., Gou, X., Wang, W., 2017. Lewis Acid Rather than Brønsted Acid Sites of Montmorillonite K10 Act as a Powerful and Reusable Green Heterogeneous Catalyst for Rapid Cyanosilylation of Ketones. Synlett 28, 439–444. https://doi.org/10.1055/s-0036-158864.

Ibrahim, Z., Koubaissy, B., Mohsen, Y., Hamieh, T., Daou, T.J., Nouali, H., Foddis, M.L., Toufaily, J., 2018. Adsorption of Pyridine onto Activated Montmorillonite Clays: Effect Factors, Adsorption Behavior and Mechanism Study. Am. J. Anal. Chem. 9, 464–481. https://doi.org/10.4236/ajac.2018.910035.

Iwamoto, R., Grimblot, J., 2000. Influence of Phosphorus on the Properties of Alumina-Based Hydrotreating Catalysts. Adv. Catal. 44, 417–503. https://doi.org/10.1016/S0360-0564(08)60516-7.

Kaur, N., Kishore, D., 2012. Montmorillonite: An efficient, heterogeneous and green catalyst for organic synthesis. J. Chem. Pharm. Res. 4, 991–1015.

Knothe, G., Kenar, J.A., 2004. Determination of the fatty acid profile by 1H-NMR Spectroscopy. Eur. J. Lipid Sci. Technol. 106, 88–96. https://doi.org/10.1002/ejlt.200300880.

Knothe, G., 2006. Analyzing Biodiesel: Standards and Other Methods. J. Am. Oil Chem. Soc. 83, 823–833. https://doi.org/10.1007/s11746-006-5033-y.

Lazlo, P., 1987. Chemical Reactions on Clays. Science 235, 1473–1477. https://doi.org/10.1126/science.235.4795.1473.

Madejova, J., Pentrak, M., Palkova, H., Komadel, P., 2009. Near-infrared spectroscopy: A powerful tool in studies of acid-treated clay minerals. Vib. Spectro. 49, 211–218. https://doi.org/10.1016/j.vibspec.2008.08.001.

Ming-Yuan, H-., Zhonghui, L., Enze, M., 1988. Acidic and hydrocarbon catalytic properties of pillared clay. Catal. Today 2, 321–338. https://doi.org/10.1016/0920-5861(88)85013-2.

Mittelbach, M., Silberholz, A., Koncar, M., 1995. In novel aspects concerning acid-catalyzed alcoholysis of triglycerides oils-fats-lipids. Proceedings of the 21st World Congress of the International Society for Fats Research, The Hague, October 1995, pp. 497–499.

Morterra, C., Magnacca, G., Demaestri, P.P., 1995. Surface Characterization of Modified Aluminas: III. Surface-Features of PO4-Doped Al2O3. J. Catal. 152, 384–395. https://doi.org/10.1006/jcat.1995.1093.

Nascimento, A. R., Alves, J. A.B.L.R., Melo, M.A.F., Melo, D.M.A., Souza, M.J.B., Pedrosa, A.M.G., 2015. Effect of the Acid Treatment of Montmorillonite Clay in the Oleic Acid Esterification Reaction. Mater. Res. 18, 283–287. http://dx.doi.org/10.1590/1516-1439.293014.

Occelli, M.L., Tindwa, R.M., 1983. Physicochemical properties of montmorillonite interlayered with cationic oxyaluminum pillars. Clay Clay Miner 31, 22–28. https://doi.org/10.1346/CCMN.1983.0310104.

Olutoye, M.A., Wong, S.W., Chin, L.H., Amani, H., Asif, M., Hameed, B.H., 2016. Synthesis of fatty acid methyl esters via the transesterification of waste cooking oil by methanol with a barium-modified montmorillonite K10 catalyst. Renew. Energy 86, 392–398. https://doi.org/10.1016/j.renene.2015.08.016.

Parr, R.G., Szentpaly, L., Liu, S., 1999. Electrophilicity Index. J. Am. Chem. Soc. 121, 1922–1924. https://doi.org/10.1021/ja983494x.

Pergher, S.B.C., Corma, A., Fornes, V., 1999. Materiales laminares pilareados: preparación y propiedades. Quim. Nova 22, 693–709. https://doi.org/10.1590/S0100-40421999000500013.

Shao, Y., Ghan, Zh., Epifanovsky, E., Gilbert, A., Wormit, M., Kussmann, J., Lange, A., Behn, A., Deng, J., Feng, X., Ghosh, D., Goldey, M., Horn, P., Jacobson, L., Kaliman, I., Khaliullin, R., Kuś, T., Landau, A., Liu, J., Head-Gordon, M., 2015. Advances in Molecular Quantum Chemistry Contained in the Q-Chem 4 Program Package. Mol. Phys. 113, 184–215. https://doi.org/10.1080/00268976.2014.952696.

Shinoda, T., Onaka, M., Izumi, Y., 1995. Proposed Models of Mesopore Structures in Sulfuric Acid-Treated Montmorillonites and K10. Chem. Lett. 24, 495–496. https://doi.org/10.1246/cl.1995.495.

Snoeyink, V.L., Jenkins, D., 1980. Water Chemistry. John Wiley & Sons, Inc., United States of America.

Spartan Software, 2018. Available online: https://www.wavefun.com/spartan.

Tan, Y.A., Oh, F.C.H., Ong, S.H., Berger, K.G., 1981. Characteristics of Malaystan palm mid fractions. PORIM Report 81, 1-18.

Tichit, D., Fajula, F., Figueras, F., Bousquet, J., Gueguen, C., 1985. Thermal Stability and Acidity of Al3+ Cross Linked Smectites. Stud. Surf. Sci. Catal. 20, 351–360. https://doi.org/10.1016/S0167-2991(09)60185-3.

Zhang, Y., Niu, S., Lu, C., Gong, Z., Hu, X., 2020. Catalytic performance of NaAlO2/γ-Al2O3 as heterogeneous nanocatalyst for biodiesel production: Optimization using response surface methodology. Energy Convers. Manag. 203,. https://doi.org/10.1016/j.enconman.2019.112263 112263.